Shear and Frictional Interactions between Adsorbed Polymer Layers in a Good Solvent

Uri Raviv, Rafael Tadmor,† and Jacob Klein*

Department of Materials and Interfaces, Weizmann Institute of Science, Rehovot 76100, Israel

Received: November 14, 2000; In Final Form: May 1, 2001

The forces between layers of poly(ethylene oxide) (PEO), of molecular weights $M = 37 \times 10^3$ (PEO37) and $M = 112 \times 10^3$ (PEO112) adsorbed onto smooth, curved solid (mica) surfaces across the good solvent toluene have been determined using a surface force balance (SFB). The SFB used is capable of measuring both normal interactions $F_n(D)$ as a function of surface separation D and, with extreme sensitivity, shear or frictional forces $F_s(D,v_s)$ between them as they slide past each other at velocity v_s. The $F_n(D)$ profiles are closely similar to those measured in earlier studies between adsorbed PEO layers. The shear or frictional forces between the sliding PEO-bearing surfaces are very low up to moderate compressions of the adsorbed layers (local pressures up to ca. 10^5 N m^{-2}), corresponding to effective friction coefficients $\mu_{eff} = (F_s/F_n)$ of order 0.003 or less. This is attributed to the fluid interfacial layer between the adsorbed layers resulting from their weak mutual interpenetration. At higher loads F_s increases markedly, and two forms of behavior are found depending on the PEO molecular weight. For PEO37, a sharp increase in F_s is followed by removal of polymer from within the intersurface gap during sliding, high friction, and adhesion between the surfaces. For the longer PEO112, the initial increase in F_s and in μ_{eff} saturates at the highest loads (for the case of μ_{eff} even decreasing), indicating that the slip plane has moved from the polymer/polymer midplane to the polymer/solid interface. The dependence of F_s on the sliding velocity in the high-friction regime is weak, suggesting that at low compressions there is a thinning of the mutual adsorbed-layer-interpenetration region at high v_s that offsets the higher viscous dissipation in that region. At the highest loads, when the slip plane has shifted to the mica surface, the weak $F_s(v_s)$ dependence is characteristic of sliding friction at solid substrates.

Introduction

Normal interactions between surfaces bearing adsorbed and grafted polymers (so-called polymer brushes) immersed in a liquid medium have direct implications for a wide range of technologies. These include colloidal stabilization and destabilization,[1,2] adhesion,[3] thin-film stability,[4−6] control of surface energies and biocompatibility,[7] and protective (anti-fouling) surface coatings in filtration applications.[8,9] Such forces have been measured over the past 20 years or so, using a variety of methods, and are reasonably well understood.[10] The surface force balance (SFB) technique in particular has been used to characterize such normal surface interactions directly in a variety of systems.[10−13] More recently, these investigations have been extended to the case of *lateral interactions*, that is, the forces that act between compressed, polymer-bearing surfaces as they slide past each other.[14] Such lateral forces control a different set of phenomena, including the issue of liquid flow past polymer-coated surfaces, and friction, wear, and lubrication effects,[15] both in man-made[16,17] and in natural and in biological systems.[7] Computer simulation studies of such interactions[18,19] have also contributed to our insight. The understanding of such frictional interactions at a molecular level is much more limited than in the case of normal forces. This is in part because of the difficulty in studying directly the very weak forces that may be associated with shear, and the consequent relative paucity of experimental data; and in part because the mechanism of shear is closely tied to dynamic and time-dependent effects, which are less easy to model than equilibrium phenomena.

Shear interactions between polymer-bearing solid surfaces have been studied in some detail for the case of polymer brushes,[20−23] and there is an emerging understanding of the mechanism that governs these forces.[14] The extremely low frictional forces that have been observed between sliding brush-bearing surfaces (with friction coefficients as low as 0.001 or less) have been attributed to the weak interpenetration between the opposing, compressed brushes even at moderately strong pressures: This results in a fluid interfacial layer between the sliding brushes even as, due to the osmotic repulsions between them in the good solvent medium, they support a large normal load. At higher loads and compressions the mutual brush interpenetration increases and, especially for brushes that become glassy at high concentrations, the frictional forces become large. The plane of slip between the surfaces may then revert from the midplane interface between the compressed brushes to that at the solid−polymer interface.[24,25]

More limited results have been reported for adsorbed polymers in near-Θ-solvents,[26] and the rheological and shear properties of (solvent-free) polymer melts confined between solid surfaces have also been studied.[27] However, shear and frictional forces for the most common case of surface-attached polymer layers, which is that of adsorbed polymers in good solvent conditions, has not to our knowledge been investigated to date, and this is the subject of the present study. In this paper we report direct measurements of the forces between two atomically smooth mica surfaces bearing adsorbed layers of

* Correspondence to Weizmann Institute of Science or to Physical and Theoretical Chemistry Laboratory, Oxford University, South Parks Road, Oxford, U.K.

† Present address: Department Chemical Engineering, University California at Santa Barbara, Santa Barbara, CA 93106.

10.1021/jp0041860 CCC: $20.00
Published on Web 08/07/2001

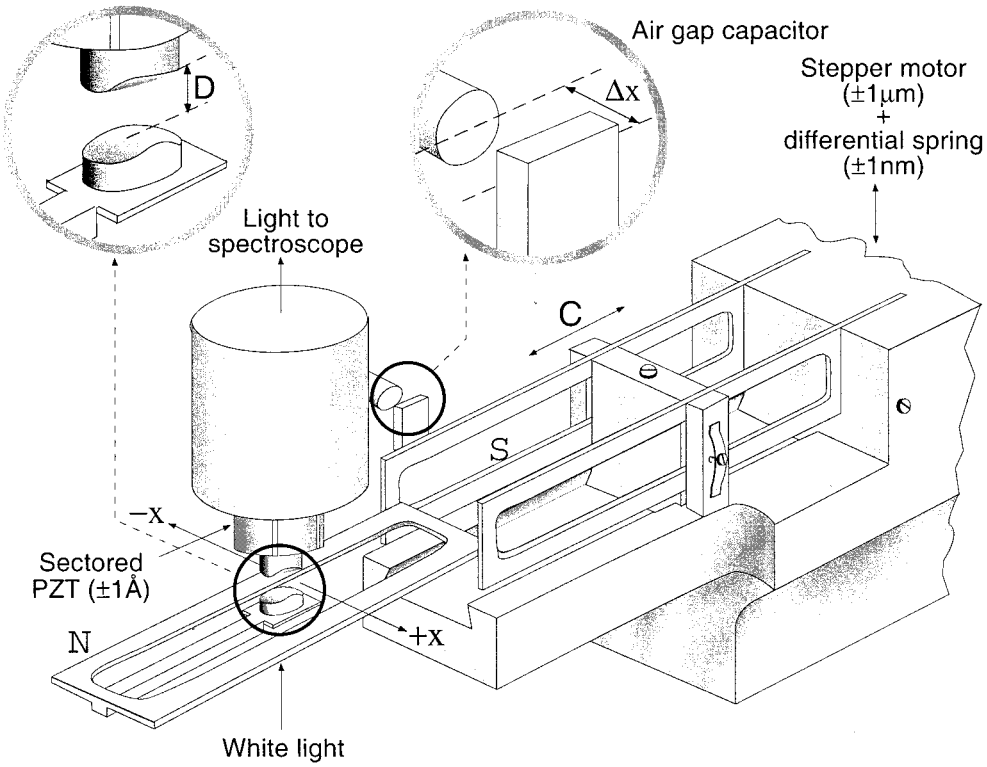

Figure 1. Schematic illustration of the surface force balance (SFB) used in the present study. Atomically smooth mica sheets are mounted on the crossed cylindrical lenses (top left inset), and their separation D is measured (to ±2 Å) using multiple beam interference and controlled (to ±2 Å) via a three-stage mechanism terminating with a sectored piezoelectric tube (PZT) on which the top surface is mounted. Lateral motion in the x direction parallel to the lower surface, which is mounted on two orthogonal springs, is also provided by the PZT (to ±2 Å). Parallelicity can be controlled via a feedback potential to the inner conducting surface of the PZT.[34b] The bending of the normal force spring N is monitored via changes in D, and that of the shear force spring S, Δx, via changes in an air-gap capacitor (to ±2 Å), top right inset. These provide a measure of normal and shear forces, respectively. The spring constant K_s of S is adjustable via a sliding clamp C (its value in the present study is set at K_s = 70 N/m). The optimal sensitivity of this SFB in measuring shear forces between the surfaces is an order of magnitude better than in a previously described version,[34b] due mainly to the improved signal-to-noise ratio arising from the present spring configuration. It is several orders of magnitude more sensitive in measuring shear stresses than scanning probe methods such as friction-force microscopy.[34b]

poly(ethylene oxide) (PEO) in the good solvent toluene. Detailed studies of the normal forces between adsorbed PEO layers both in toluene and in water under good solvent conditions have been reported earlier,[28−31] and we extend these to the case of shear forces between the compressed, adsorbed layers. We use PEO of two molecular weights M. While common features are observed at low to moderate compressions, we find significant differences between the behavior of the long and the short adsorbed chains under shear, when the load (and friction) are high. In particular, the data indicate that the low M polymer is removed from the intersurface gap in these conditions, while the high M material remains between the surfaces but appears to slide along the solid substrate. This behavior is reminiscent of low- and high-M polystyrene brushes sliding under high compressions.[24,25] In the following sections we describe the experimental procedure and the results, focusing on the different behavior at the two M values, and in the Discussion we consider the mechanisms that may be responsible for the frictional behavior.

Experimental Section

Methods. The SFB technique and detailed experimental procedures have been described earlier.[32,33] The present force balance, incorporating in particular both normal and shear force measuring capabilities, shown schematically in Figure 1, is a modification of that described in detail earlier[22,34b] but has considerably greater resolution and sensitivity.[34a] This is due to a different mounting of the normal and shear force springs, which considerably reduces the noise in the shear force signal due to ambient vibrations.

To recall briefly: two-half-silvered mica sheets (thickness ca. 2 μm and atomically smooth on both sides) are mounted opposite each other on upper and a lower cylindrical lenses in a crossed-cylinder configuration (equivalent to a sphere on a flat). White-light multiple beam interferometry reveals the distance D between them (to ±0.1−0.2 nm) and the geometry of the contact region (including the mean radius of curvature R = ca. 1 cm). Fine motion in both normal (D) and lateral (x) directions is provided by a sectored piezoelectric tube (PZT), as described in the caption to Figure 1. The normal and shear forces F_n and F_s are determined directly from the bending ΔD and Δx, respectively, of the two orthogonal springs, as $F_n = K_n \Delta D$ and $F_s = K_s \Delta x$, where K_n = 100 N/m and K_s = 70 N/m are the respective spring constants. In addition, it is possible to measure the refractive index $n(D)$ of the medium separating the surfaces.

The resolution and sensitivity in the shear force measurement is noise-limited and is optimally $\delta F_s = \pm 50$ nN. The noise is due to ambient vibrations that are transmitted despite the electronic vibration isolation system. The circuitry of the air gap capacitor may also introduce some high-frequency electronic noise. By using an XYt plotter to record the shear response traces, much of the high-frequency electronic noise is suppressed, because the plotter is a mechanical system that is unable to follow the high frequencies. Surface separation D can be changed either by the application of normal motion, using the

TABLE 1: Molecular Characteristics of the Polymer Samples

polymer	$10^{-3}M_w$	M_w/M_n	R_g (nm)
PEO37	37	1.07	6.2
PEO112	112	1.04	10.7

differential motor or the PZT (Figure 1) or by utilizing the occasional slow motion of the surfaces toward each other, which results from dimensional changes due to thermal drift.

Materials. The ethanol and toluene used for cleaning were supplied by Bio-Lab Inc. (Jerusalem) and were analytical grade. The toluene used for the measurements was hypersolvent grade for HPLC 99.8% (BDH Laboratory) and used as received. The mica was ruby muscovite, grade 1, supplied by S & J Trading Inc. (New York). The PEO used, terminated with a hydroxyl group and used as received, was supplied by Polymer Laboratories Ltd., Church Stretton, U.K. The molecular characteristics of the polymers used (Table 1) were determined by GPC and light scattering (manufacturers' data).

Procedure. Before every experiment, glassware was cleaned by immersion in $K_2CrO_4-H_2SO_4$ for ca. 10 min and rinsed with deionized water followed by water obtained from a water-purification system (ELGA) and filtered ethanol. Tools, glassware, and the parts of the SFB coming in contact with the toluene were sonicated for ca. 10 min in toluene and rinsed with filtered ethanol. After cleaning the aparatus and mounting the mica sheets onto the lenses using sucrose as glue, at the first stage in each experiment the surfaces are brought into contact in air (to determines the $D = 0$ position) and the shear response is calibrated. The surfaces are then separated (to ca. 2 mm) and the box is filled with toluene. After allowing 1 h for thermal equilibration, a normal force−distance profile, $F_n(D)$, is taken. This is usually the point where impurities can be detected. Only experiments free of impurities are taken to the next stage. PEO was dissolved in toluene by heating the solution to 35−40 °C for ca. 5 min, and the PEO solution, in concentrations of either 40 ± 5 or 100 ± 5 μg/mL, was introduced by replacing the pure solvent with the polymer solution, while keeping a gap of 2 mm between the surfaces within which a liquid meniscus was maintained. Polymer was allowed to adsorb onto the surfaces for an incubation time of 12−16 h (at 2 mm separation), the polymer adsorbed to the surfaces and $F_n(D)$ profiles were determined. Uniform back and forth shear motion was then applied to the top mica surface via the PZT, and the lateral force $F_s(D)$ between them was recorded over a range of surface separations D by monitoring the bending of the shear springs. $F_n(D)$ profiles were measured regularly following shear measurements in order to check the effect of shear on the adsorbed layer. The mean radius of curvature R of the mica sheets at each contact position is determined from the shape of the interference fringes.

Results

The results described below are based on at least four separate experiments (different pairs of mica sheets) for each PEO molecular weight.

Pure Toluene. In each experiment, prior to introducing the PEO solution, normal $F_n(D)$ profiles were measured between the bare mica surfaces immersed in pure toluene, to check for the absence of contamination as noted. Results measured on both compression and decompression are shown in Figure 2, where the force axis is normalized as $F_n(D)/R$: in the Derjaguin approximation (for $R \gg D$) $F_n(D)/2\pi R$ is the corresponding interaction energy $E(D)$ per unit area between two flat parallel surfaces, a distance D apart obeying the same force−distance law.[35]

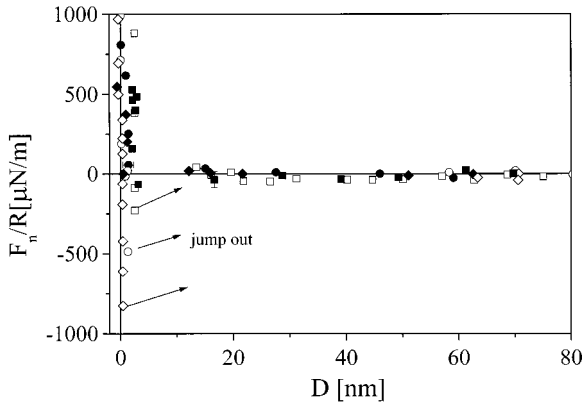

Figure 2. Normal force (F_n)−distance (D) profiles between curved mica surfaces in pure toluene, where the force axis is normalized as (F_n/R) (R = mean radius of curvature of the mica) to yield the interaction energy per unit area between flat parallel plates obeying the same $F_n(D)$ law, in the Derjaguin approximation.[35] Different symbols indicate different sets of experiments. Solid symbols are used for force profiles measured during compression of the two surfaces, while open symbols indicate force profiles measured during decompression.

This normalization enables comparison of $F_n(D)/R$ profiles from different experiments and is used in all subsequent normal and shear force profiles. No forces were detected for $D > 5$ nm, below which the surfaces came into adhesive contact ($D = 1 \pm 1$ nm), in agreement with previous studies.[30] On separation the surfaces jump out (to a position where no forces are acting between them), due to a mechanical instability expected whenever $\partial F_n(D)/\partial D > K_n$, the constant of the normal forces spring. The form of the interaction may be suggestive of some water condensation between the surfaces; we did not examine in detail the possible presence of structural forces,[36] though the scatter of both repulsive and adhesive forces may indicate the presence of such effects. The main point is that the attraction indicated the absence of contaminants in the polymer-free system, while its range is small compared with the range of interactions once polymer had adsorbed. This simplifies subsequent interpretation of the results.

Following addition of the PEO solution at concentrations of either 40 ± 5 or 100 ± 5 μg/mL, the surfaces were allowed to incubate in the solution overnight at separation of 2 mm. Normal force profiles were then determined prior to the shear measurements both to ensure absence of contamination and as a control following shear.

Normal Forces. Figures 3 and 4 show the normal force profiles for PEO37 and PEO112, respectively.

These profiles are quantitatively similar to those observed in earlier studies for the identical system of PEO adsorbed from toluene onto mica.[30] For comparison, we show in Figure 3 (PEO37) as solid lines, curves that best fit to the results in PEO, $M_w = 40$k of Luckham and Klein;[30] the quantitative agreement is quite close. The main features are as follows: on initial compression, a monotonic repulsion commences at a range of several R_g ($7.3 \pm 0.8R_g$ for PEO37 and $8.8 \pm 0.5R_g$ for PEO112): this defines the onset separation $D = 2L$, where L is the equilibrium thickness of each adsorbed layer. On decompression immediately following close approach, the forces are considerably shorter ranged, probably indicating the forced adsorption of more segments onto the mica surface and a transient compressive distortion of the adsorbed layers. On

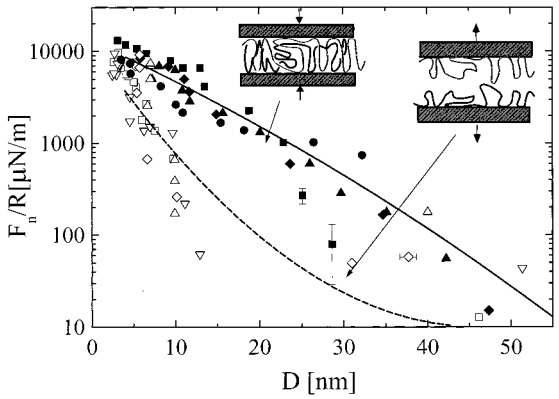

Figure 3. Normalized force−distance profiles, (F_n/R) vs D, following overnight incubation of the mica surfaces in 40 and 100 μg/mL solution of PEO37 in toluene. Measurements during compression and rapid decompression of the two surfaces are shown in different sets of experiments, with the insets illustrating the motion. Different symbols refer to different contact positions at different mica sheets. Solid symbols indicate forces measured during compression, and open symbols indicate forces measured during decompression. We note that the profiles on a recompression immediately following a decompression are identical, within the scatter, to the original compression profile. The results are compared with curves summarizing the results of Lucham and Klein for PEO (M_w = 40 000) in similar conditions.[30]

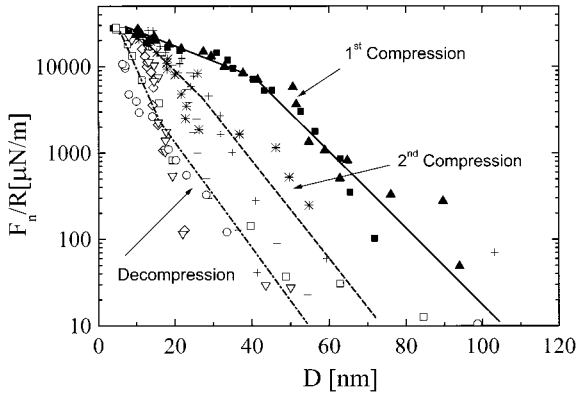

Figure 4. Normalized force−distance profiles, (F_n/R) vs D, following overnight incubation of the mica surfaces in 100 μg/mL solution of PEO112 in toluene. Measurements during first compression and subsequent rapid decompression/compression cycles are shown in different sets of experiments. Different symbols refer to different contact positions at different mica sheets. Solid symbols indicate forces measured during compression, and open symbols indicate forces measured during decompression. The cross-like symbols represent forces measured during the second compression. The solid and broken lines are a guide to the eye.

subsequent recompression the layers relax back to their original (equilibrium) structure to an extent depending on the molecular weight and the time to the recompression: for PEO37, full relaxation occurs even for "immediate" recompression (within 10 min following the first approach run, Figure 3). For PEO112 the relaxation on immediate recompression is partial, and full relaxation to the equilibrium $F_n(D)$ profile occurs only after about 1 h. These features are very similar to those observed earlier,[30] including, in particular, the shorter relaxation times for the more rapidly relaxing shorter PEO chains. The issue of partial relaxation on recompression following a first approach is relevant to the question of the effective friction coefficient between the sliding layers, discussed below.

Shear Forces. Shear forces between the compressed PEO-covered surfaces in the respective polymer solutions were measured by applying uniform back and forth shear motion,

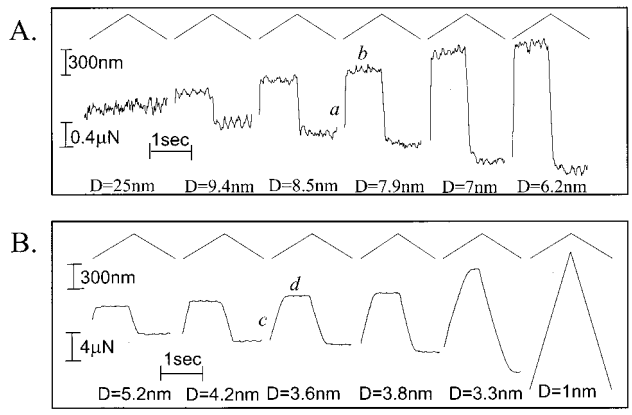

Figure 5. (A and B) Shear forces between mica sheets bearing adsorbed PEO37 in PEO37/toluene solution, as the surfaces slide past each other, at different surface separations D as indicated. Each pair of traces monitors the uniform back and forth lateral displacement applied to the upper surface, as a function of time (top trace within each pair) together with the shear force transited to the lower surface (bottom trace within each pair). We show data collected at different contact positions from two different mica sheets. We present only one period of the shear response at each separation, but we note that each one of the responses repeated itself several times as long as D remained the same. In the a and c regimes there is both bending as well as sliding of the shear spring (see text). In the b and d regimes the surfaces are sliding freely past each other, while the magnitude of the forces in these regimes, which are due to bending of the shear springs (lower traces within each pair) represent the sliding or kinetic friction force. Scales of time, shear forces, and lateral displacement are indicated on the traces.

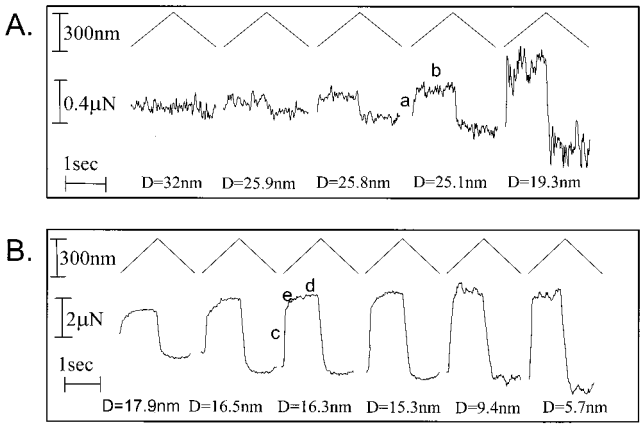

Figure 6. (A and B) As in Figure 5, but for sliding of mica surfaces bearing adsorbed PEO112 in PEO112/toluene solution.

amplitude ca. 300 nm, at frequency 0.5 Hz, to the top surface, and monitoring the resultant bending of the shear spring on which the lower surface is mounted. Measurements were carried out starting from the onset of normal repulsion and at decreasing separations D down to strong compressions. Figures 5 and 6 show the shear forces F_s transmitted to the lower surface in response to the applied lateral back and forth motion Δx_0 of the top surface, as the surfaces approach smaller separations, for the adsorbed PEO37 and PEO112 layers, respectively. The traces are reproduced directly from the XYt recorder.

Qualitatively, the behavior for both molecular weights is similar up to moderate compressions: no frictional forces are measurable above the noise level δF_s in the signal as the surfaces are compressed down to separations that are substantially smaller than $2L$. The initial regime where F_s becomes measurable is shown in Figures 5A and 6A: for both PEO37 and PEO112, shear forces are first detected at compression ratios ($2L/D$)

greater than about 4, that is, at $D \lesssim 10$ nm and $D \lesssim 26$ nm, respectively. At higher compressions the shear forces transmitted to the lower surface, as the top surface moved back and forth, progressively increased. We note that at the onset of detectable shear force (at $D = D_o$) the pressure P between the surfaces, for the PEO112 case, is given by[21] $P = P(D_o) = (1/(2\pi R))(\partial F/\partial D)_{D_o} \approx 1 \times 10^5$ N m^{-2}.

The protocol for the shear force measurements is as follows: A normal compression−decompression run was carried out to ensure integrity of the layers just prior to the shear measurements. The surfaces were then enabled to approach slowly by thermal drift as the top surface moved laterally, while D was monitored simultaneously from the position of the interference fringes. As seen in Figures 5 and 6, the initial response to shear is a rise in F_s (regions a or c in the shear traces), followed by a plateau region (b or d in the traces). In general, the applied lateral motion Δx_0 is related to the sliding between the surfaces, of extent $\Delta x_{\text{sliding}}$, and to the bending of the lower shear spring, of extent Δx, as $\Delta x_0 = \Delta x_{\text{sliding}} + \Delta x$ (we recall that the traces show $F_s = K_s \Delta x$). In the rise regions (a and c in the traces), $\Delta x_{\text{sliding}}$ represents the extent to which the opposing PEO layers slide past or disentangle from each other as the top surface rubs past the lower one; it is of order 80% of Δx_0 when F_s first becomes measurable (lower compressions), decreasing to ca. 20% of Δx_0 at the higher compressions. The extent of sliding increases toward the top of the rise region. At the top the shear force equals the frictional resistance, and steady sliding takes place (regions b and d in the traces): the magnitude of F_s in this plateau region at the different compressions is the kinetic friction force for this shear velocity.

We note that at the higher compressions there is a qualitative difference between the frictional response with PEO37 and between that for the PEO112 layers. For the shorter polymer (PEO37, Figure 5B), the force increases strongly and monotonically, and the surface separations D become smaller than the closest approach attainable on normal compression alone. At the closest separations, $D = 1 \pm 0.5$ nm or so, the static frictional force exceeds the shear force and there is no sliding between the surfaces: They remain in rigid contact as the top surface moves laterally (right-hand trace in Figure 5B). This approach almost to contact is an indication that at the highest compressions PEO37 has been removed from the contact zone by shear, as directly confirmed below by $F_n(D)$ profiles taken after the shear. For the longer chains (PEO112, Figure 6B), the frictional forces at the highest compressions rise much less sharply and, indeed at the strongest compressions appear to be almost constant (four right-hand traces in Figure 6B). The extent of sliding toward the top of the rise region is larger at the higher molecular weight (region e in the traces 6B compared to traces 5B). This may imply that the longer chains were first stretched to a larger extent (compared to the shorter chains) before steady sliding occurred**.** These different behaviors are highlighted in Figures 7 and 8, where the plateau values of F_s (the kinetic friction) are plotted against surface separation for the two polymers, based on traces as in Figures 5 and 6.

We note that while F_s in the case of the shorter polymer increases monotonically and exponentially with decreasing D, the kinetic friction for the case of the longer polymer appears to level out for $D <$ ca. 15 nm. Also shown as solid curves in Figures 7 and 8 are the appropriate compression profiles for the two polymers, to indicate the variation in normal load as the surfaces compress. As noted, the shear profiles were measured while approaching the surfaces following a compression run and separation: the solid curves are therefore the

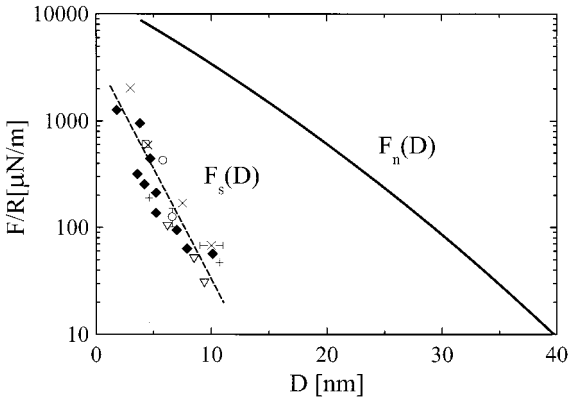

Figure 7. Variation of the shear forces $F_s(D)$ (normalized by the radius of curvature R) between curved mica surfaces bearing adsorbed PEO37 in PEO37/toluene solution, sliding past each other, and taken from traces as in Figure 5 (at sliding velocity v_s of ca. 300 nm/sec as in Figure 5), as a function of their separation D. The magnitude of F_s shown is in all cases from the freely sliding region of each trace. Also shown, solid curve, is the normal force profile (F_n/R) measured during compression of the surfaces, based on the data of Figure 3. Different symbols refer to different contact positions or experiments. The shear forces are below the detection limit for $D \gtrsim 10$ nm.

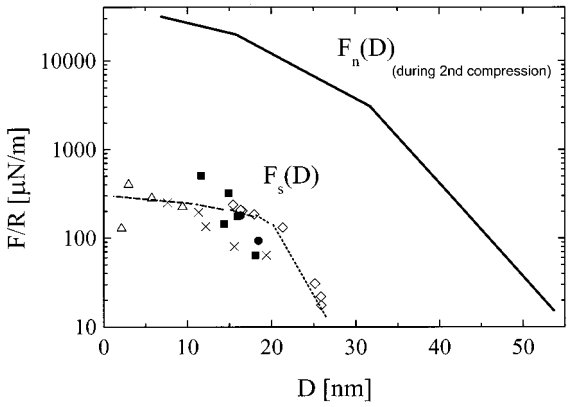

Figure 8. Variation of the shear forces $F_s(D)$ (normalized by the radius of curvature R) between curved mica surfaces bearing adsorbed PEO112 in PEO112/toluene solution, sliding past each other and taken from traces as in Figure 6 (at sliding velocity v_s of ca. 300 nm/sec as in Figure 6), as a function of their separation D. The magnitude of F_s shown is in all cases from the freely sliding region of each trace. Also shown, solid curve, is the normal force profile (F_n/R) measured during the second compression of the surfaces following compression and separation, based on the data of Figure 4. Different symbols refer to different contact positions or experiments. The shear forces are below the detection limit for $D \gtrsim 26$ nm.

corresponding $F_n(D)$ profiles for the two polymers. For PEO37, recompression following compression is similar to the first compression; while for PEO112, the solid curve in Figure 8 represents the second recompression profile. Because the shear itself changes the nature of the normal interactions (particularly for PEO37, see below), the solid curves serve as a reliable guide to the load, once shear measurements have been made, only for the regime of moderate compression (prior to the onset of measurable shear forces). We may define an effective kinetic friction coefficient $\mu_{\text{eff}} = F_s(D)/F_n(D)$. If we take the magnitude of F_n just at the onset of measurable F_s to be its value from the $F_n(D)$ profiles, and the magnitude of F_s at that point to be $\Delta F_s \approx 0.1$ μN at most, we find that at the onset point, $\mu_{\text{eff}} \lesssim 0.003$ for both the PEO37 and PEO112 data.

Normal Forces Following Shear. At the end of each of the shear runs (which lasted some 15 min from start to finish in the case of PEO37 and up to 1 h for PEO112) the surfaces were

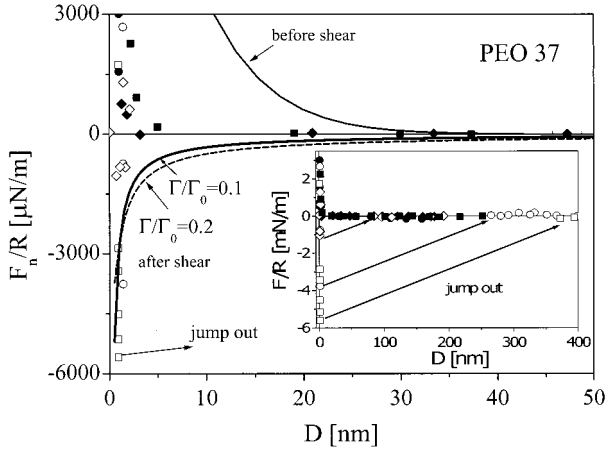

Figure 9. Normalized force−distance profiles (F_n/R) vs D following shear measurements between PEO37-bearing mica surfaces. Measurements from different sets of experiments taken during compression and decompression of the two surfaces are shown. Different symbols refer to different contact positions on different mica sheets. Solid symbols indicate forces measured during compression, and open symbols indicate forces measured during decompression. We indicate with the arrow (and show in the inset over a wider range of data) that on separation the surfaces jumped out to a far distance (zero force region). For comparison, normal force profiles, before shear, are presented as the top solid curve (based on the profiles in Figure 3). The lower solid line is the force−distance profile calculated[47] for adsorbing PEO in water at 10% surface coverage and the dashed line is for 20% surface coverage (see text). Inset: The same force profiles with identical symbols, but here we included the range to which the surfaces jump out, when the pulloff force exceeds the adhesion. At each of the force−distance profiles the maximum applied load under compression was different: the extent of the jumpout, proportional to the adhesive force, increased with increasing maximum load or load-time prior to pulloff. These forces should be compared with those between polymer-free surfaces in pure toluene, Figure 2.

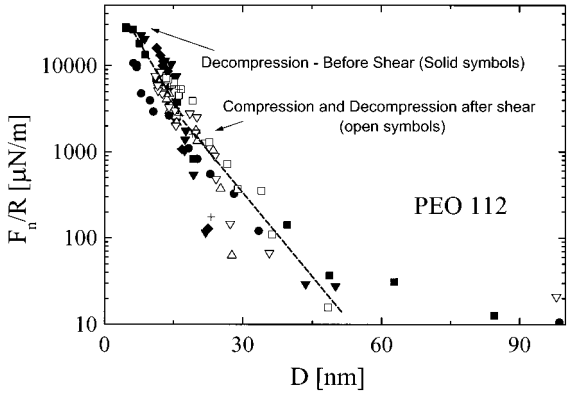

Figure 10. F/R vs D profiles following shear measurement between PEO112-bearing mica surfaces. Different symbols refer to different contact positions or different mica sheets. Solid symbols indicate forces measured during compression and open symbols indicate forces measured during decompression. For comparison, $F(D)/R$ profiles measured during decompression, before shear, are presented in the dashed line (based on the profiles of Figure 4).

taken apart. In the case of the PEO37 layers, the surfaces were strongly adhered at the end of the shear run ($D \approx 0.5-1$ nm) and jumped out, on separation, to some $2-3$ μm, while in the case of PEO112 they moved out smoothly under a monotonically decreasing repulsion. To obtain further insight, we carried out a number of controls. $F_n(D)$ profiles taken immediately after the shear runs reveal the state of the adsorbed layers, and are shown in Figures 9 and 10 for PEO37 and PEO112, respectively.

As clearly seen in Figure 9, the $F_n(D)$ profile for PEO37 is very different to its form prior to the shear: it shows a short-ranged repulsion (at $D \lesssim 3$ nm) on approach of the surfaces, and a marked attraction on separating the surfaces following compression, when jump-outs occur, as shown in the inset. The magnitude of the attraction is greater than for bare mica surfaces in toluene (Figure 2), and we also note that it increases with the time of compression and to some extent with the magnitude of the compression itself (inset to Figure 9). Comparison of the before-shear and after-shear $F_n(D)$ profiles, Figure 3 vs Figure 9, clearly shows that much of PEO37 has been removed from between the surfaces by the shear. The dependence of the adhesive strength on the compression time prior to separation further suggests that the adhesion is due to residual polymer chains bridging the gap and that with time of compression more segments are forced onto the surfaces, resulting in stronger bridging. The solid and broken lower curves in Figure 9 are the theoretically predicted bridging attractions (discussed in the following section) for interaction between surfaces bearing 10% and 20% of the equilibrium adsorbance of PEO in a good solvent. Both the much-reduced separation for onset of repulsion on compression (2.5 ± 0.5 nm) and the marked bridging adhesion thus indicate that a substantial part of PEO37 has been removed from the surfaces during the shear run.

In contrast, the normal force profiles for PEO112, Figure 10, resemble much more their pre-shear forms, except that both compression and decompression following shear resembled the decompression profiles prior to shear. This may indicate that a few of the longer PEO chains were removed from between the surfaces during the friction measurements, or that the shear caused a distortion of the adsorbed layers, which causes their relaxation to be more sluggish (or a combination of both). Supporting the latter idea is the fact that it took over 2 h following a shear run for the PEO112 layers to fully relax to their equilibrium $F_n(D)$ behavior (with onset at ca. 100 nm), twice as long as for full recovery following compression prior to shear.

We note in passing that experiments carried out at concentration of 40 ± 5 μg/mL showed no significant difference from the experiments performed at 100 ± 5 μg/mL.

For the case of PEO37 we carried out a further control experiment. The PEO37 solution was replaced with pure toluene (except for a meniscus between the surfaces), diluting it by a factor of ca. 1000, and $F_n(D)$ profiles were determined to confirm equilibrium behavior. Shear motion was then applied as before, following which normal force profiles were again measured. These were identical (within the scatter) to the $F_n(D)$ profiles taken after shear in the solution (Figure 9). Then the surfaces were kept at a separation of ca. 20 μm for 2 days to enable relaxation of chains on the surface. $F_n(D)$ profiles taken at various points during this period were similar to the $F_n(D)$ profiles measured immediately after shear. This sequence of measurements demonstrates directly that in the pure toluene, once the PEO37 chains had been removed by shear, there was no recovery of the contact position, even after 2 days, suggesting that polymer from adjacent parts of the mica did not migrate along the mica to heal the sheared region. The pure toluene was then replaced with the PEO solution, and the surfaces held at separation of ca. 20 μm for 5 days, to limit the rate of polymer adsorption.[37] Normal force profiles measured at various points during this period showed gradual recovery of the PEO-adsorbed layer, clearly due to adsorption of new PEO37 chains from the solution.

Variation of Shear Forces with Sliding Velocity. This was examined for the case of the PEO112 layers only (as the shorter polymer was known to be removed from the gap on shear).

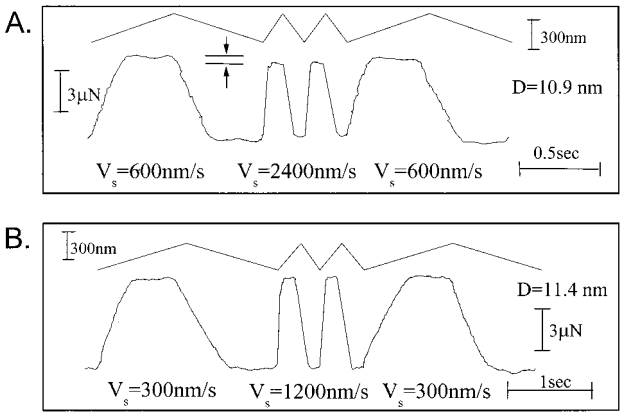

Figure 11. (A and B) Shear forces (lower traces in each of A and B) between mica surfaces bearing adsorbed PEO112 in PEO112/toluene solution, measured by applying a back and forth lateral motion at velocity v_s to the top surface (top traces), at different velocities, as indicated, for two different surfaces separations. The motion was applied at a given v_s, then v_s was changed and finally returned to its original value.

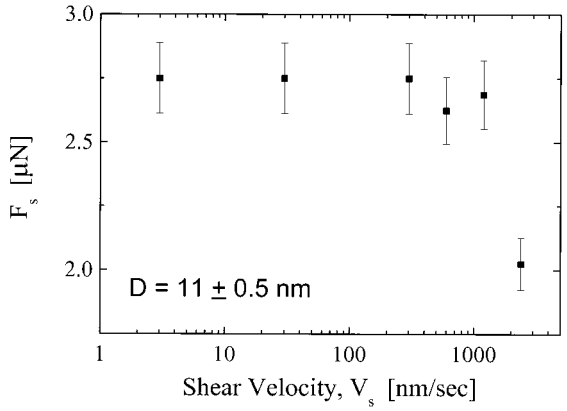

Figure 12. Variation of the shear forces F_s between mica surfaces bearing adsorbed PEO112 in PEO112/toluene solution, as a function of shear velocity v_s, at $D = 11$ nm, taken from profiles such as in Figure 11.

For this, back and forth lateral motion, at different velocities, was applied on the top surface in three stages, under constant load. At the first stage the motion was applied at a certain velocity, then the shear velocity was changed and at the final stage the original velocity was applied again. Thus, the reversibility of the shear response at the original velocity was tested. In Figure 11, typical applied lateral motion and shear force response traces of the three stages are presented in two different sets of velocities, at a surface separation in the range ($D <$ ca. 15 nm, Figure 6) at which the friction forces increase only weakly. Within the uncertainty in F_s, the amplitude of the shear response did not change with increasing shear velocity in this separation range, up to a velocity ~2400 nm/s (for this separation), as shown in Figure 12.

At this velocity the shear response appeared to decrease by about ~15%. This behavior, shown in Figure 12 for $D = 11$ nm, was found also at larger separations (up to $D = 18$ nm).

Discussion

The main new findings of this study are that the adsorbed PEO in the good solvent medium strongly modifies the shear forces between compressed, sliding surfaces. It results initially, up to moderate compressions, in a striking reduction of the friction, similar to that between polymer brushes in a good solvent,[14] though differing markedly from the behavior of adsorbed chains in a Θ-solvent where frictional drag sets on almost as soon as normal forces are detected.[26] At higher compressive loads between the surfaces, the behavior depends on the PEO molecular weight. In the case of the shorter chains (PEO37), the polymer is removed from the contact region by the shear, accompanied by a sharp, monotonic increase in the friction. For the longer chains (PEO112) on the other hand, a more moderate increase in the friction appears almost to saturate at higher loads, and little further increase occurs at the highest compressions attained in our study.

Before analyzing this behavior in more detail, we note that the normal force profiles $F_n(D)$ prior to shear (and after equilibrium is attained after shear) resemble very closely, both qualitatively and quantitatively, the behavior observed in the earlier study by Luckham and Klein.[30] A long-ranged repulsion on approach, followed by a shorter ranged repulsion on separation, which has been attributed to a transient "higher-than-equilibrium" adsorption onto the surfaces of the compressed polymer. This reverts with time to the original $F_n(D)$ profile as the adsorbed layer relaxes to its equilibrium conformation, more rapidly for the PEO37 chains (indeed on recompression the original compression profile is retrieved), and more slowly for the longer chains, as also observed in the previous study. In view of an earlier controversy concerning the presence of dust particles in leading to aggregation of PEO in solution,[38,39] and the role of filtration in suppressing this, it is of interest that our results, where the polymer solutions were unfiltered , closely resemble the earlier Luckham/Klein study[30] where filtration was used.[40] Finally, in anticipation of later discussion, we recall that the dependence of the normal forces F_n on surface separation D has been considered in detail previously.[41] We note here only the variation in the highly compressed regime,[29,30,41] for which $(F_n/R) \propto D^{-\alpha}$, where $\alpha = 1-1.25$; the exponent arises from the variation of osmotic pressure with segmental concentration in the intersurface gap.

PEO Adsorbance. The amount of polymer adsorbed on the interacting surfaces is an important parameter for understanding the frictional behavior. Since the refractive index of PEO is very similar to that of toluene, we could not measure the adsorbance Γ from refractive index measurements, as was done for the case of PEO in water for example.[29] We may, however, estimate it from the force profiles, as in the earlier PEO/mica/toluene studies.[30] In the high compression regime ($D <$ 20 nm for PEO37 and $D <$ 30 nm for PEO112), we assume that the polymer is uniformly distributed in the gap between the surfaces, thus $\phi_{gap} \approx 2\Gamma v/D$, where v is the specific volume of the polymer (0.89 cm^3/g). The pressure between the plates is then equal to the osmotic pressure in the gap $\Pi(\phi(D))$. The change in the surface energy by going from D_1 to D_2 is given by

$$\Delta E = E(D_1) - E(D_2) \approx \int_{D_2}^{D_1} \Pi(\phi(D))\, dD \qquad (1)$$

and $\Pi(\phi(D)) = -k_B N_A T/v_1\{\ln(1-\phi) + \phi + \chi\phi^2\}$, where v_1 is the molar volume of the toluene (106.5 cm^3/mol ($\rho = 0.865$ g/cm^3, $M_w = 92.14$)), which is a good approximation (within a numerical prefactor of order unity) at the high polymer concentration in the gap at high compression. Solving the integral, we obtain

$$\{F(D_1) - F(D_2)\}/R = -2\pi k_B N_A T/v_1\{(D_2 - 2\Gamma v)\ln(1 - 2\Gamma v/D_2) - (D_1 - 2\Gamma v)\ln(1 - 2\Gamma v/D_1) + \chi(2\Gamma v)^2(1/D_1 - 1/D_2)\} \quad (2)$$

Using the experimental data, we estimate $\Gamma_{PEO37} \approx 0.9 \pm 0.2$ mg·m^{-2} and $\Gamma_{PEO112} \approx 1.3 \pm 0.3$ mg·m^{-2}. These values are close to those estimated, using the same approach, in the earlier Luckham/Klein study[30] (where, for example, Γ_{PEO40} was estimated as 1 mg/m^2). In practice, while the functional form of the expression for the osmotic pressure is correct, in absolute terms it is probably correct only within a numerical prefactor of order unity.[42,43]

Shear Interactions between Sliding Adsorbed Layers. A striking feature of our results concerns the low shear forces required to slide the PEO-bearing surfaces past each other, and the correspondingly low effective friction coefficient μ_{eff}, observed at compression ratios $\beta \lesssim 4$ for both PEO samples ($\beta \equiv 2L/D$, where $2L$ is the separation at onset of repulsion). Similarly, low friction has been observed in the case of mutually compressed, sliding polymer brushes,[14] though in that case the low friction (below the measurement resolution) persisted up to even greater compression ratios, $\beta \approx 8$. We believe the origin of the low friction is qualitatively similar in both brush-like and adsorbed surface layers in good solvent media: As the opposing layers are compressed, they experience a large osmotic repulsion due to excluded volume effects, while the extent of interpenetration remains relatively weak. For the case of compressed polymer brushes, the extent $d_{brush}(D)$ of interpenetration as the brush-bearing surfaces are compressed to a separation D varies rather weakly,[14,44,45] as $d_{brush}(D) \propto D^{-1/3}$; that is, an 8-fold compression from initial overlap will merely double $d_{brush}(D)$. This results in little entanglement in the interpenetration zone, a correspondingly fluid interfacial layer, and thus a low friction coefficient.

For the case of interpenetrating adsorbed layers one expects, merely from the power law shape of the concentration profile[46] $\phi = \phi(0)(a/z)^{4/3}$, that there should be greater interpenetration of the compressed adsorbed polymers at moderate compressions than for the compressed parabolic concentration profile brushes.[45] This is because the increase in monomer concentration at the brush edge (parabolic profile) is much sharper than the power-law tail at the extremity of the adsorbed layers. Indeed, the 4-fold compression from initial overlap of the adsorbed layers to the point where strongly rising frictional forces are first observed (as opposed to 8-fold for brushes) suggests this is qualitatively the case.

For compression ratios greater than 4 the shear forces begin to rise markedly. This is due to the drag on the mutually interpenetrating moieties from opposing layers within the overlap zone $d_{adsorbed}(D)$, as illustrated in Figure 13A.

The drag is related to the effective viscosity η_{eff} within the overlap zone. At increasing compressions two effects occur. First, $d_{adsorbed}(D)$ increases as greater interpenetration occurs (until the entire gap may be permeated by chains from both surfaces), and at the same time the mean monomer concentration (or volume fraction ϕ) within this zone, and throughout the gap, increases as $\phi = 2\Gamma\upsilon/D$, thereby increasing η_{eff} and the frictional drag. These effects both contribute to the increasing F_s at smaller D. As the shear behavior of the PEO37 and PEO112 chains is rather different at the highest compressions, it is appropriate to consider them separately. For PEO37, the data show clearly that the chains are removed from the gap by the shear. This implies that the lateral forces on the PEO37 chains are sufficient to desorb them from the adsorbing mica surface and that under the strong compression they are squeezed out from between the region of closest approach due to the lateral outward pressure gradient resulting from the curved area of contact. This happens only for the PEO37 chains, which presumably have a higher mobility than the PEO112 chains due to their relatively low molecular weight. As chains desorb and move away, surface sites on the adsorbing substrate are released, and bridging by the remaining chains is enhanced, particularly as the surface separations at which this happens are much smaller than the equilibrium adsorbed layer thickness or R_g of the chains. The bridges resist lateral motion due to being stretched, as illustrated in Figure 13B, and as this is a progressive process (the more chains desorb, the more bridges, the greater the resistance to lateral sliding), the friction increases sharply with decreasing separation, as shown in Figure 7. The final situation is one where the few PEO37 chains that remain on the surface are strongly bridging, resulting in the marked adhesion between the surfaces manifested in $F_n(D)$ profiles following shear (Figure 9).

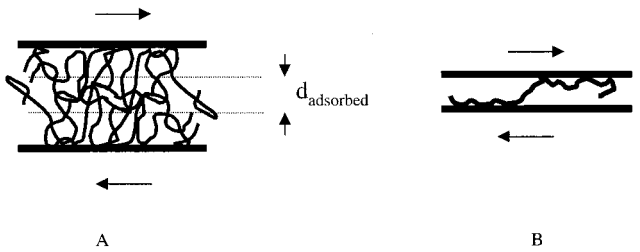

Figure 13. (A) Schematically showing the zone of mutual interpenetration $d_{adsorbed}$ between compressed, sliding surfaces bearing adsorbed polymers. Viscous dissipation which results in the sliding friction between the surfaces takes place entirely within $d_{adsorbed}$. The extent of this zone increases with compression until it may occupy the entire gap, and in addition, $d_{adsorbed}$ may decrease on rapid sliding as chains are pulled out of it. (B) Schematic representation of a single chain bridging the gap between two sliding surfaces, indicating how at low adsorbance (resulting, for example, from chain pulloff) such bridging can lead to strong frictional resistance as the chain is dragged past the surfaces.

We may try to estimate roughly the number of chains remaining on the surfaces in two ways. First, by fitting to the prediction of a recent model[47] on interactions between surfaces bearing a subequilibrium adsorbance of chains in a good solvent. This model enables the forces between surface-adsorbed polymers in a good solvent to be calculated in terms of experimentally observable parameters, such as bulk osmotic pressures in the corresponding polymer solution, and the single surface segment-density profile (determined for example by neutron scattering). Using appropriate parameters,[48] we generated the two lower attractive profiles in Figure 9 corresponding to adsorbances of 10% and 20% of the equilibrium value; the attraction is basically due to bridging by the polymer dominating the interactions at low adsorbance. While these profiles do not describe the short-range repulsion on approach (filled data points in Figure 9), suggesting equilibrium bridging is not fully developed, they are roughly in the range of the adhesive forces on separation, once bridging has taken place following the compression. The other indication is from the range of interactions on approach and compression, where the surfaces approach to separations of ca. 1 ± 0.5 nm at the highest compressions, indicating a maximal adsorbance of ca. $30 \pm 10\%$ of its value prior to shear. Thus, we estimate that some $80 \pm 10\%$ of PEO37 is removed by the shear.

For the case of PEO112, the initial shear response is similar. Frictional drag is due to viscous dissipation within an interpenetration zone whose extent $d_{adsorbed}(D)$ increases at smaller D, while the concentration dependent η_{eff} also increases. This results in the initial increase in F_s observed as D decreases (Figure 8). However, the leveling off of this increase for $D < D_c \approx 15$ nm suggests a different mechanism is emerging: In analogy with what has been suggested for strongly compressed

polymer brushes,[24,25] we believe this change is due to the shift or crossover of the plane of slip from the *midplane* between the surfaces, i.e., the middle of the interpenetration zone, to the *polymer/substrate* interface, when F_s becomes large enough. The reason is that the resistance to sliding is then smaller for dragging monomers past the substrate than it is for sliding chains through each other.

We may explore this idea as follows. We first assume the overlap region extends over most of the intersurface gap, so that for $D \lesssim D_c$, $d_{adsorbed}(D) \approx D$, and that the polymer concentration is uniform in the gap. The mean volume fraction of polymer at the crossover separation is $\phi(D_c) = 2\Gamma v/D_c$, and the viscosity of a bulk PEO(M) solution at this concentration would be $\eta(M,\phi(D_c))$. We should bear in mind that the polymers are all attached to one surface or the other, so that it is not in general valid merely to apply the Newtonian relation for shear stress σ_s across sliding surfaces a distance D apart moving at velocity v_s and separated by a fluid of (Newtonian) viscosity η,

$$\sigma_s = (v_s/D)\eta \tag{3}$$

It would be more correct to evaluate the drag on the interpenetrated PEO moieties as the two adsorbed layers slide through each other, as has been done for the case of polymer brushes,[14] but this requires a more detailed molecular consideration than is within the scope of the present paper. We proceed therefore with eq 3, bearing in mind its limited applicability: In particular, as we are ignoring the constraints on the mobility of the PEO chains resulting from their adsorption to the two surfaces, using the straightforward Newtonian expression in eq 3 must result in a weaker shear stress than would be the case if such constraints were taken into account. Putting $D = D_c = 15$ nm and typical values of v_s ($v_s = 300$ nm/s, e.g., as for traces in Figure 6), with $\eta(112k,\phi(D_c))$ estimated from literature values,[49] we find $\sigma_s \approx 10^3$ N/m^2. We convert this to the shear force expected over the effective contact area A_{eff} given by the Hertzian contact mechanics[50] expression, $A_{eff} \approx \pi(RF_n/K)^{2/3}$, where $K \approx (1 \pm 0.3) \times 10^9$ N/m^2. Thus, A_{eff} is typically of the order 3×10^{-10} m^2, at the F_n value corresponding to D_c (Figure 4), and $F_s = \sigma_s A_{eff} \approx 0.3$ μN at that separation. Bearing in mind our discussion and the approximations above, this value, while lower than that observed, $F_s(D_c) \approx 2\mu$N (from Figure 6 or 8), is certainly in line with our expectations.

To evaluate the force needed to drag the adsorbing monomers past the surface, we assume that a fraction (a/D_c) of the monomers in the gap are adsorbed in contact with the surface (equivalent to assuming a uniform monomer distribution in the gap[43]), where a is the monomer size. The number of adsorbing monomers/unit area is then $n_{ads} = \phi(D_c)/a^2$. The shear force required to detach a monomer from the surface is roughly ϵ/δ, where ϵ is the adsorption energy per monomer (the adsorption energy for PEO on mica from a moderately good solvent has been estimated[47] as $(\epsilon/a^2) \approx 0.1$ kT/nm^2) and $\delta \approx 1$ Å is the extent by which the monomer−substrate (dipole−dipole) bond must be stretched to rupture and detach from the mica. From these considerations, we have the total shear stress to detach all adsorbing monomers as $\sigma_{s,\,detach} = n_{ads}(\epsilon/\delta)$, and total shear force to detach as $F_{s,detach} = \sigma_{s,detach}A_{eff}$. Putting in the relevant values this gives $F_{s,detach} \approx 100$ μN. This is about 50 times larger than the value of F_s at the point where we believe surface sliding commences. However, this calculation has explicitly made two improbable assumptions. First, because of the chain flexibility it is certain that not all monomers in contact with the surface will need to be detached at once, and in practice a dislocation-like mechanism (or waves of detachment) is likely to be active, whereby only a fraction of the monomers are detached at any instant. Second, we have assumed that all the sticking energy ϵ is dissipated, and this too is unlikely to be correct for monomers hopping laterally from one site to the other. Incorporating these factors would result in a shear stress for sliding, requiring a much weaker force than we have calculated, consistent with our expectation.

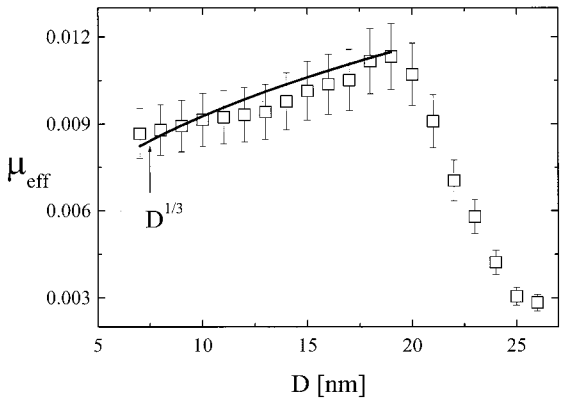

Figure 14. Variation of the effective kinetic friction coefficient $\mu_{eff} = (F_s/F_n)$ with surface separation D for sliding, PEO112-bearing mica surfaces in PEO112/toluene solution. Values of F_s and F_n taken from average profiles based on Figures 8 and 4, respectively, where the error bars represent the scatter in the data points used to generate the average values. The solid curve is the variation $\mu_{eff} \propto D^{1/3}$.

Once the plane of slip has shifted to the polymer solid surface, a further increase in the normal load results in little change to the stress required to slide the surfaces past each other. This is because the magnitude of the monomer−substrate dipolar interaction is largely insensitive to pressure, as is also the sliding mechanism described above. This is basically the reason F_s stops rising rapidly at $D < D_c$. One still expects an increase due to the progressive flattening of the region of contact A_{eff} at higher pressures, in accord with the Hertzian equation, i.e., $F_s \propto (F_n)^{2/3}$, and this is the broken curve indicated for $D < D_c$ (= 15 nm) in Figure 8. The corrolary is that the effective friction coefficient for $D < D_c$, given by $\mu_{eff} = (F_s/F_n)$, decreases as $F_n^{-1/3}$ at decreasing loads. If we assume, as earlier noted,[46] that in the high compression regime $(F_n/R) \propto D^{-1}$, then this at once gives a relation between the effective friction coefficient μ_{eff} and the surface separation in our experiments: $\mu_{eff} \propto D^{1/3}$. In Figure 14 we plot the variation of μ_{eff} vs D for PEO112, from the data in Figure 8; we see clearly the crossover in μ_{eff} at $D \approx D_c$, while the solid line, corresponding to $\mu_{eff} \propto D^{1/3}$, describes well its decrease at closer separations. This supports well our idea of the transition from midplane to substrate sliding of the compressed adsorbed layers at high compressions.

Velocity Dependence of Shear Forces. We note the very weak variation of the shear forces with shear velocity v_s in the region $D < D_c$ (where the plane of shear has shifted to the polymer/solid interface), as seen in Figure 12 over nearly 3 decades in v_s. The reason for this is that the frictional dissipation occurs not at the midplane via viscous drag of the interpenetrated moieties, which would have a much higher (liquid-like) v_s dependence, but rather by sliding of the monomers along the substrate. The velocity dependence of such a sliding process resembles solid−solid friction, which is well-known to be only very weakly velocity dependent.[16,51]

Finally, for the case where $D \gtrsim D_c$, where we also observed a rather weak v_s dependence of the shear force despite the fact that dissipative processes at the midplane are expected to be active, the underlying reason is different. It is because at higher

shear velocities the extent of mutual interpenetration zone (the magnitude of $d_{adsorbed}$, Figure 13A) is diminished as surfaces slide more rapidly. Essentially, one expects the relaxation rate of the interpenetrated moieties to roughly equal the shear rate ($v_s/d_{adsorbed}$) within the interpenetration zone,[52] so that higher shear rates correspond to shorter interpenetrated chain sections. Thus, the increased viscous dissipation within this zone is offset by the reduction in its thickness, and this, we believe, is the origin of the weak dependence of the shear force on the sliding velocity.

Conclusions

We have carried out for the first time a systematic study of the frictional forces between two solid surfaces bearing adsorbed polymers in a good solvent medium, the most common case of surface coverage by polymers, for two polymers (PEO37 and PEO112) differing significantly in molecular weight M. Our results reveal that the polymers can reduce friction strikingly, to effective friction coefficients of ca. 0.003 or less under moderate pressures (up to pressures $\approx 1 \times 10^5$ N.m^{-2}). This results from a combination of being able to support a large load due to osmotic repulsion between the compressed layers in the good solvent medium, while at the same time the sheared interfacial zone within which the frictional dissipation occurs remains rather fluid. At higher pressures the frictional behavior depends on M. For the shorter chains (PEO37) our data show that chains are detached from the surfaces and squeezed out from the intersurface gap, and the friction rises sharply, suggesting that increased bridging occurs. For the higher M polymer (PEO112) the friction initially increases at higher compressions but then saturates. This occurs because the plane of slip at the higher loads reverts from the midplane to the polymer−surface substrate, while at the same time the more entangled longer chains do not have sufficient mobility to escape the gap as did the shorter ones. Our results have interesting implications for the use of adsorbed polymers as lubricants, and suggest that high M polymers will better serve than low M ones, as they are more likely to remain within the gap during sliding at higher friction.

Acknowledgment. We thank Tom Witten for useful discussions and the Minerva Foundation, the US−Israel BSF, and the Deutsches-Israel Program (DIP) for support of this work. We also thank the Eshkol Foundation for a studentship to U.R.

References and Notes

(1) Fleer, G. J.; Cohen-Stuart, M. A.; Scheutjens, J. M. H. M.; Cosgrove, T.; Vincent, B. *Polymers at Interfaces*; Chapman and Hall: London; 1993.

(2) Napper, D. H. *Polymeric stabilization of colloidal dispersions*; Academic Press: London; 1983.

(3) Lee, L. H. *Fundamentals of Adhesion*; Plenum: New York, 1991.

(4) Leger, L.; Joanny, J. F. *Rep. Prog. Phys.* **1992**, *55*, 431.

(5) Yerushalmi-Rozen, R.; Klein, J. *Langmuir* **1995**, *11*, 2806.

(6) Yerushalmi-Rozen, R.; Klein, J.; Fetters, L. J. *Science* **1994**, *263*, 793.

(7) *Proc. Inst. Mech. Eng. part H: Engineering in Medicine* **1987**, *210*, Special Issue on Biolubrication.

(8) Koehler, J. A.; Ulbricht, M.; Belfort, G. *Langmuir* **1997**, *13*, 4162.

(9) Sung, L. K.; Morris, K. E.; Taylor, J. S. *Desalination Water Reuse* **1994**, *38*,.

(10) Luckham, P. F. *Colloid Interface Sci.* **1996**, *1*, 39.

(11) Eiser, E.; Klein, J.; Witten, T. A.; Fetters, L. J. *Phys. Rev. Lett* **1999**, *82*, 5076.

(12) Leckband, D. E.; Israelachvilli, J. N.; Schmitt, F. J.; Knoll, W. *Science* **1992**, *255*, 1419.

(13) Patel, S.; Tirrell, M. *Annu. Rev. Phys. Chem.* **1989**, *40*, 597.

(14) Klein, J. *Annu. Rev. Mater. Sci.* **1996**, *26*, 581.

(15) Dan, N. *Colloid Interface Sci.* **1996**, *1*, 48.

(16) Bowden, F. P.; Tabor, D. *The Friction and Lubrication of Solids II*; Clarendon Press: Oxford, U.K., 1964.

(17) Briscoe, B. J. *Philos. Magn.* **1981**, *43*, 511.

(18) Grest, G. S. *Phys. Rev. Lett.* **1996**, *76*, 4979.

(19) Neelov, I. M.; Borisov, O. V.; Binder, K. *J. Chem. Phys.* **1998**, *108*, 6973.

(20) Granick, S.; Demirel, A. L.; Cai, L. L.; Peanasky, J. *Isr. J. Chem.* **1995**, *35*, 75.

(21) Klein, J.; Kumacheva, E.; Mahalu, D.; Perahia, D.; Fetters, L. *Nature* **1994**, *370*, 634.

(22) Klein, J.; Perahia, D.; Warburg, S. *Nature* **1991**, *352*, 143.

(23) Schorr, P.; Kilbey, S. M.; Tirrell, M. *Polym. Prepr. (Am. Chem. Soc., Div. Polym. Chem.)* **1999**, *218*, *278-POLY, Part 2 AUG*, U477.

(24) Klein, J. In *Interactions, friction and lubrication between polymer-bearing surfaces*; Bhushan, B., Ed.; Kluwer Academic: Amsterdam, 2000; pp 177−198.

(25) Klein, J.; Kumacheva, E.; Perahia, D.; Fetters, L. J. *Acta Polym.* **1998**, *49*, 617.

(26) Klein, J.; Kumacheva, E.; Perahia, D.; Mahalu, D.; Warburg, S. *Faraday Discuss.* **1994**, *98*, 173.

(27) Luengo, G.; Schmitt, F. J.; Hill, R.; Israelachvili, J. *Macromolecules* **1997**, *30*, 2482.

(28) Klein, J.; Luckham, P. F. *Nature* **1984**, *308*, 836.

(29) Klein, J.; Luckham, P. F. *Macromolecules* **1984**, *17*, 1041.

(30) Luckham, P. F.; Klein, J. *Macromolecules* **1985**, *18*, 721.

(31) Luckham, P. F.; Klein, J. *J. Chem. Soc., Faraday Trans.* **1990**, *86*, 1363.

(32) Israelachvili, J. N.; Adams, G. E. *J. Chem. Soc., Faraday Trans. 1* **1978**, *79*, 975.

(33) Klein, J. *J. Chem. Soc., Faraday Trans. 1* **1983**, *79*, 99.

(34) (a) First results using this version of the SFB (though without providing a description) were reported by Eiser et al. in ref 11. (b) Klein, J.; Kumacheva, E. *J. Chem. Phys.* **1998**, *108*, 6996.

(35) Derjaguin, B. V.; Churaev, N. V.; Muller, V. M. *Surface Forces*; Plenum Publishing Corp.: 1987.

(36) Christenson, H. K. *J. Chem. Phys.* **1983**, *78*, 6906.

(37) Almog, Y.; Klein, J. *J. Colloid Interface Sci.* **1985**, *106*, 33.

(38) Klein, J.; Luckham, P. F. *J. Colloid Interface Science* **1990**, *141*, 593.

(39) Marra, J.; Hair, M. L. *J. Colloid Interface Sci.* **1988**, *125*, 552.

(40) This suggests that PEO/toluene in the study where PEO was unfiltered, and where marked aggregation was observed,[39] may have been affected by nucleating particles present in their PEO samples, which had a different provenance to the present material.

(41) de Gennes, P. G. *Macromolecules* **1982**, *15*, 492.

(42) From a comparison with an earlier study of PEO adsorbed on mica from aqueous electrolyte,[29] where absolute values of the adsorbance were obtained from refractive index profiles and could also be obtained using the above approach from the $F_n(D)$ profiles, we may conclude that the prefactor is somewhat larger than unity. Its upper limit in our case is of order 1.5 since the distance of closest approach at highest compression of the adsorbed layers would correspond to adsorbances of 1.5 and 2 mg/m^2 for the PEO37 and PEO112 layers, respectively, assuming no chains are squeezed out of the gap by the normal forces.

(43) de Gennes, P. G. *Scaling Concepts in Polymer Physics*; Cornell University Press: Ithaca, NY, 1979.

(44) Wijmans, C. M.; Zhulina, E. B.; Fleer, G. J. *Macromolecules* **1994**, *27*, 3238.

(45) Witten, T.; Leibler, L.; Pincus, P. *Macromolecules* **1990**, *23*, 824.

(46) de Gennes, P. G. *Macromolecules* **1981**, *14*, 1637.

(47) Klein, J.; Rossi, G. *Macromolecules* **1998**, *31*, 1979.

(48) To calculate the curves in Figure 9, we used parameters corresponding to the water/PEO system.[47]

(49) From *Poly(ethylene oxide)* (by F. E. Bailey and J. V. Koleske, Academic Press, New York, 1976), we have the viscosity η of a 5% solution of PEO ($M = 10^5$) $\approx$ 0.02 Pa s. Using the empirical relation $\eta = (\text{const})\phi^{5.4}M^{3.4}$ for entangled polymer solutions (*Polymer Handbook*, 4th ed.; Brandrupp, Immergut, Eds.; Wiley: New York) and the volume fraction $\phi(D_c) = 2\Gamma v/D_c \approx 0.2$, we estimate $\eta(1.12 \times 10^5, \phi(D_c)) \approx 50$ Pa s.

(50) Johnson, K. L.; Kendall, K.; Roberts, A. D. *Proc. R. Soc. (London), Ser. A* **1971**, *324*, 301.

(51) Bowden, F. P.; Tabor, D. *The Friction and Lubrication of Solids I*; Clarendon Press: Oxford, U.K., 1950.

(52) Tadmor, R.; Janik, J.; Klein, J. Submitted for publication.